Semiconductor Physics, Quantum Electronics & Optoelectronics, 2024. V. 27, No 4. P. 397-403.

Semiconductor physics

Numerical estimations of the maximal distance of target detection in the IR spectrum with decreasing the target–background temperature contrast

Ye.O. Melezhyk, Z.F. Tsybrii, V.V. Zabudsky, N.I. Kukhtaruk*, V.V. Strelchuk, A.S. Nikolenko, O.F. Kolomys, V.I. Popenko, D.M. Maziar, M.A. Alieksandrov, P.M. Lytvyn

V. Lashkaryov Institute of Semiconductor Physics, NAS of Ukraine
41 prosp. Nauky, 03028 Kyiv, Ukraine
**Corresponding author e-mail: KukhtarukN@gmail.com*

Abstract. This paper discusses the distance limit of target detection in the infrared (IR) spectrum for targets with different temperatures. Numerical estimations of the relative decrease in the maximum detection range (MDR) with a decreasing temperature contrast of the target relative to the background (ΔT) are presented. It is shown that an order-of-magnitude decrease in ΔT leads to a decrease in the MDR by approximately one-third, while a two-order-of-magnitude decrease in ΔT results in an approximately two-thirds decrease in the MDR. Estimates of the MDR were carried out for favorable and unfavorable weather conditions. These results are relatively valid for both the 3…5 and 8…12 μm spectral ranges and seem to be independent of weather condition.

Keywords: IR, thermal contrast, maximum detection range.

https://doi.org/10.15407/spqeo27.04.397
PACS 07.57.-c, 42.30.Lr, 42.30.Va

Manuscript received 16.09.24; revised version received 13.10.24; accepted for publication 13.11.24; published online 06.12.24.

1. Introduction

Nowadays, applications of infrared radiation in reconnaissance and target detection are widely studied and addressed by numerous scientific groups [1–5]. Observation within the infrared range allows one to see hot targets at relatively large distances, in adverse weather conditions, and even *via* areas of smoke, dust, or fog where visual detection becomes inapplicable. Detection within the infrared spectrum allows one to track effectively not only targets like moving aircraft but also various ground vehicles and even personnel.

Due to the high atmospheric absorbance of IR radiation within the prevailing part of its spectrum, target detection is possible only in so-called atmospheric transmittance windows – for radiation wavelengths 3…5 μm and 8…12 μm [6]. Nevertheless, even in these windows, IR radiation is absorbed by the atmosphere, and its intensity decreases with the distance.

The detection distance limits for thermal imagers depend on their spatial resolution and the temperature difference ΔT between the target and the background. Therefore, one of the important engineering tasks for combat vehicles is their thermal masking or thermal camouflage, which leads to the minimization of thermal contrast ΔT between the vehicle and the background. The minimization of the thermal contrast causes a decrease in the distance at which the vehicle can be reliably detected using a thermal imager (Maximum Detection Range) [7].

Commercially available matrix thermal imagers differ greatly in their characteristics, namely in Noise-Equivalent-Temperature-Difference (NETD), matrix resolution, and camera field of view defined by lens parameters and sensor size. High-resolution imagers are very expensive and not always available for engineers who develop or investigate thermal signature reduction. Therefore, it is important to develop a simple theoretical algorithm for qualitative estimation of the MDR at different ΔT. Calculating the MDR with a given ΔT for several high-resolution thermal imagers, one can evaluate the masking properties of a thermal camouflage [8].

Thermal imagers are characterized by minimal thermal and spatial resolution. While the NETD of a certain imager is usually given by its manufacturer, things are much more complicated with spatial resolution. One of its core concepts is the so-called Modulation Transfer Function (MTF), which describes the degradation of on-screen image contrast compared to the contrast of observed objects. This function depends on the target spatial frequency and is usually not provided by the manufacturer, making pure theoretical calculations of the MDR for a particular thermal imager very erroneous. In the next section, we will introduce a mixed experimental and mathematical apparatus used for these calculations.

© V. Lashkaryov Institute of Semiconductor Physics of the NAS of Ukraine, 2024
© Publisher PH "Akademperiodyka" of the NAS of Ukraine, 2024

2. Theory

According to NATO standard STANAG 4347 [9], there are three characteristics describing the thermal imagers: Maximum Detection Range (MDR), Maximum Recognition Range (MRR), and Maximum Identification Range (MIR). Detection of a target is a probabilistic event, strongly depending on target observation time and operator qualification. Thus, STANAG 4347 defines these ranges for a 50% probability of an appropriate event, assuming that the operator has infinite time to make observations using the well-known Johnson criteria [10]:

- detection – corresponds to 1 line pair per target;
- recognition – corresponds to 3 line pairs per target;
- identification – corresponds to 6 line pairs per target.

Atmospheric gases have highly non-uniform IR emission and absorption spectra. Thus, to calculate the attenuation of irradiation passing through the atmosphere, one can use sophisticated line-by-line or statistical narrow-band approaches based on the actual absorption spectrum [11]. However, due to the requirement of simplicity and the significance of other sources of calculation errors, it is often good enough to use an approximation of gray gas with a uniform absorption coefficient.

The STANAG 4347 assumes that despite the different absorption spectra within the transmittance windows 3…5 and 8…14 μm, radiation attenuation occurs with a uniform absorption coefficient and is described by simple exponential decay. As absorption strongly depends on actual weather, it is assumed that the absorption coefficient σ is equal to 0.2 km^{-1} for good transmission conditions and 1 km^{-1} for limited transmission conditions.

The standard uses the concept of minimum resolvable temperature difference (MRTD) as an integral value influenced by imager optics, matrix resolution, fields of view, and other limiting factors in the thermal imager scheme. The MRTD can be either numerically estimated or directly measured. The measurements allow us to account an actual weather/illumination conditions on the test polygon, however, they are very time-consuming and need to be done very carefully due to many sources of possible errors [12]. The MRTD is measured depending on the target spatial frequency, which can be easily converted into the distance at the fixed target dimensions.

The MRTD measurements are usually carried out on a 4-bar test pattern, and detection is considered successful when an observer can distinguish all 4 bars, regardless of how noisy they are on the screen. Therefore, these measurements are quite subjective [13] as different people can have differences in their sight. It is generally accepted in the literature that these measurements should be carried out by several observers, no less than 3 [13]. Even in this case, the differences between measurements of several teams carried out with the same equipment could vary sufficiently due to different training of personnel or weather conditions. For a detailed procedure of the MRTD measurements, please refer thorough description in [13].

The STANAG 4347 method for determining the MDR, MRR, and MIR is based on finding the distance where attenuated in atmosphere target thermal contrast ΔT becomes equal to the imager MRTD at the corresponding spatial frequency.

Distinguishing between the detection, recognition, and identification is performed according to the Johnson criteria because for the different events, we have different relations of the spatial frequency to the distance:

$$R_{det} = V_t \nu, \tag{1}$$

$$R_{rec} = \frac{V_t \nu}{3}, \tag{2}$$

$$R_{ind} = \frac{V_t \nu}{6}, \tag{3}$$

where the distance R is measured in km, while the spatial frequency ν – in $mrad^{-1}$. Here V_t is measured in meters and defines a critical (smallest) target dimension [14], for ground vehicles, this is usually height. However, in the STANAG 4347, the preset target vehicle dimensions (2.3 m per 2.3 m) are used. When vehicle dimensions are unknown, or it is hard to distinguish the main frame of a vehicle with mounted auxiliary equipment, it is convenient to use NATO standard-defined dimensions. It leads us to the equation of a thermal imager distance [9, 14] in the form:

$$\Delta T e^{-\sigma R} = \mathrm{MRTD}(\nu). \tag{4}$$

It is worth noting, there are approximate analytical formulae for calculation MRTD, like this [14]:

$$\mathrm{MRTD}(\nu_x) = \frac{0.66\,\mathrm{SNR}\,(P_r)\,\mathrm{NETD}\,\nu_x}{M_s(\nu_x)} \sqrt{\frac{\alpha_D \beta_D}{\Delta f t_0\, f_f\, t_E}}, \tag{5}$$

where SNR is the detection probability dependent on the signal-to-noise ratio, NETD is the thermal imager noise-equivalent temperature difference, f_f is the thermal imager frame rate, α_D and β_D are the field of view in horizontal and vertical dimensions, t_E – is the human eye integration time, while $\Delta f t_0 = \pi/4$ relation is often valid. Here, M_s stands for MTF. However, the practical use of this equation is limited because manufacturers of thermal imagers rarely provide the values of MTF. Consequently, various approximations of MTF can be used, for example, ignoring the modulation transfer functions of the optical system and electronic circuit of the imager. Another common simplification, in this case, is using the analytical MTF defined for a single-point detector.

In engineering calculations, such a set of undefined parameters and assumptions often could lead to sufficient errors in the numerical modeling of MRTD. Particularly, it was, when we numerically calculated the found in literature experimentally measured MRTD.

Therefore, our approach in this article is different – we use two present in the literature experimental measurements of the MRTD within 3…5 and 8…12 μm ranges and apply them to the calculation of MDR for different targets. The additional thing that should be

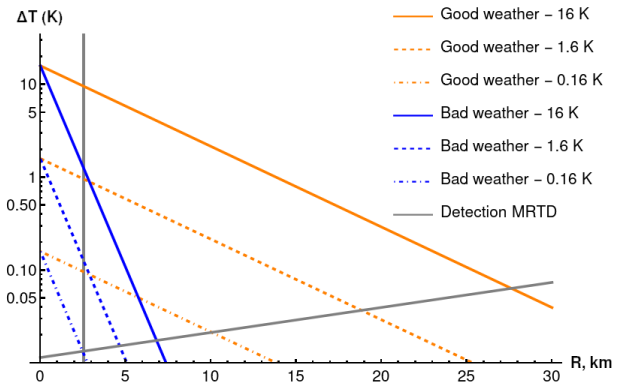

Fig. 1. Numerical determination of the MDR for 3…5 μm thermal imager. For interpretation of the colors in the figure(s), the reader is referred to the web version of this article.

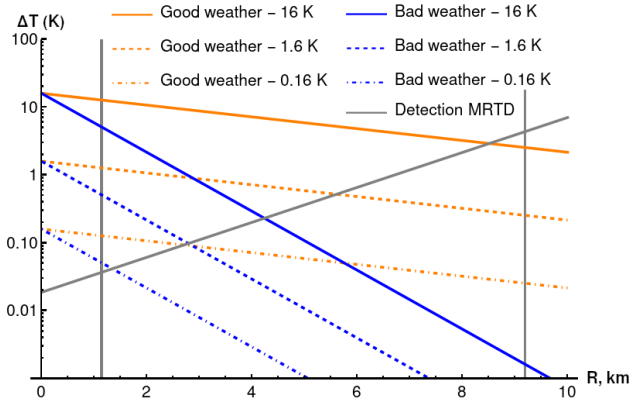

Fig. 2. Numerical determination of the MDR for 8…12 μm thermal imager.

accounted for here is the spatial resolution of imagers limited by their Nyquist frequency (the Nyquist frequency determines the thermal imager theoretical limit [13]). In practice, this means that when fitting the experimentally calculated MRTD points to a curve, we should not rely on the approximated MRTD beyond the set of experimental points either for small or large spatial frequencies.

It is worth noting that as we use for our modeling two measurements made with two particular models of thermal imagers, it would serve no purpose to talk about absolute ranges. Therefore, in the evaluation of calculated ranges, we propose to consider only their relative changes with changing the target contrast ΔT or weather conditions. Hence, we can assume that the relative changes of MDR could be qualitatively applied to thermal imagers of other models within the range of distances, where detection is not limited by the imager spatial resolution.

3. Experimental data and results of modeling

For our modeling, we used two experimentally measured sets of MRTD. The first one [4] was measured within the spectral range of 3…5 μm for a camera with an InSb matrix and 640×480 resolution. The NETD of this camera is better than 20 mK, while its field of view is 0.75°(H) × 0.56°(V). For this camera, the MRTD varied within 13…0.428 mK, while the spatial frequency lies within 1.11…24.82 mrad^{-1}. The second set of MRTD measurements [13] was done for the spectral range of 8…12 μm with the camera Marico no 232, which had the field of view 2°×1.5°, while the NETD of this camera is unknown. For this camera, the MRTD varied within 50 mK…2.3 K, while the spatial frequency lies within 0.5…3.51 mrad^{-1}.

It is worth noting that when we speak about the target temperature contrast with the background ΔT, this value is measured at such distance to the target where the target can be considered as a point source, assuming the atmospheric absorption is still very low and can be neglected.

We started with the benchmark calculations, intended to reveal how two orders of magnitude change in ΔT reflects in the change of the MDR. We used three ΔT: 16, 1.6, and 0.16 K. These particular temperature contrasts were chosen because they fit well the interval where the MRTD for both experimental data sets is not limited by neither the NETD nor the spatial resolution. For the modeling, we used a target size of 2.3 m according to the STANAG NATO standard [9]. We assumed that the actual NETD limiting experimental MRTD corresponds to a leftmost experimental point in each data set. Regarding the spatial resolution limitations for the 3…5 μm thermal imager, there is enough data to calculate the Nyquist frequency. For the 8…12 μm thermal imager there is not enough data to calculate its Nyquist frequency, thus we suggested that the spatial frequencies smaller than a rightmost experimental point frequency of 4.0 mrad^{-1} are not limited by the spatial resolution. In the following figures, vertical gray lines denote these smallest and biggest frequency/distance limits, between which the approximated curve based on experimental MRTD data can be considered reliable.

From Figs 1 and 2, we can find how the MDR changes when the temperature difference between the target and the background changes by two orders of magnitude, for good and limited weather conditions. These plots present the graphical solutions of the thermal imager equation (2) for three temperature contrasts – 16, 1.6, and 0.16 K – for good and adverse weather conditions. MDR for each case can be found as the distance R corresponding to the intersection point of a particular ΔT and MRTD curves. For the 3…5 μm range thermal imager (Fig. 1), the particular MDR values for good weather are 27.6, 18.8, and 10.1 km. The MDR values for adverse weather conditions are 6.84, 4.66, and 2.55 km. In this plot, the distance corresponding to the Nyquist frequency is well above 50 km. Within the 8…12 μm spectral range (Fig. 2), the particular MDR values for good weather are 8.5, 5.6, and 2.7 km. The corresponding MDR values for adverse weather conditions are 4.24, 2.8, and 1.35 km.

Thus, lowering the temperature difference ΔT between the target and background by an order of magnitude within 3…5 μm leads to a decrease in MDR by 32% both for good and limited weather conditions. The lowering of ΔT within this spectral range by two orders of magnitude leads to a decrease in MDR by 63%, also equally for good and adverse weather conditions.

Repeating the same calculations for the 8…12 μm thermal imager, we obtained that the decrease in ΔT by one order of magnitude leads to the decrease in MDR by 34% both for good and bad weather conditions, while the decrease in ΔT by two orders of magnitude leads to the decrease in MDR by 68% for all weather conditions.

From presented numerical results one could assume, that the relative decrease of MDR should not depend on weather conditions at all. Fig. 3 presents the simulated dependences of MDR decrease *vs* background–target ΔT lowering for two thermal imagers. One can see that the slope of the MDR dependences in the given scale will be different for different weather conditions.

It is worth noting again, that the STANAG [9] framework was developed with the assumption of uniform background temperature, which well applies to conditions met by the US Army, for example, in the desert. Thus, the obtained benchmark values correspond to the ideal observation conditions. Variations in the background temperature will make the task of target detection more complicated.

One can assume that the provided relative values of decrease in MDR can serve as an approximate benchmark for the effectiveness of various thermal signature reduction devices developed to hide both vehicles and personnel from infrared reconnaissance.

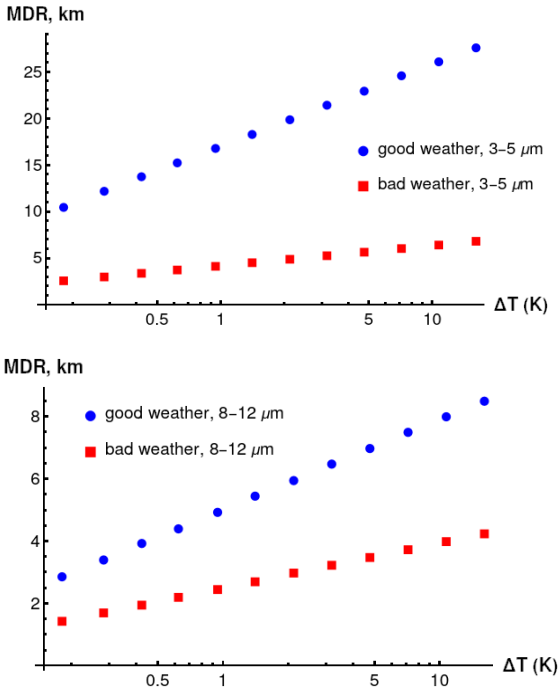

Fig. 3. Simulated dependences of the MDR decrease *vs* background-target ΔT lowering for two thermal imagers of 3…5 μm (a) and 8…12 μm (b) spectral ranges.

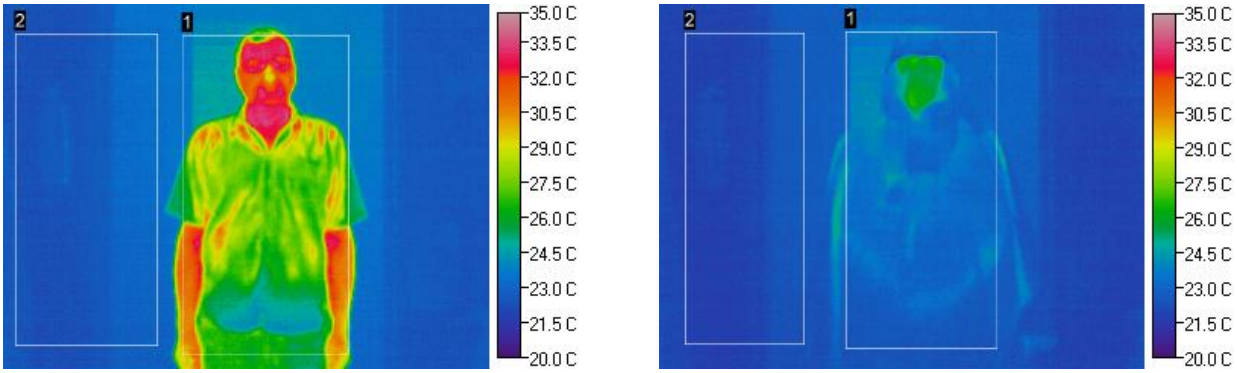

(a) (b)

Fig. 4. Thermal images of a person without (a) and with (b) thermal masking clothes. Figures allow one to determine the ΔT between the human body and the background, in both cases. For interpretation of the colors in the figure(s), the reader is referred to the web version of this article.

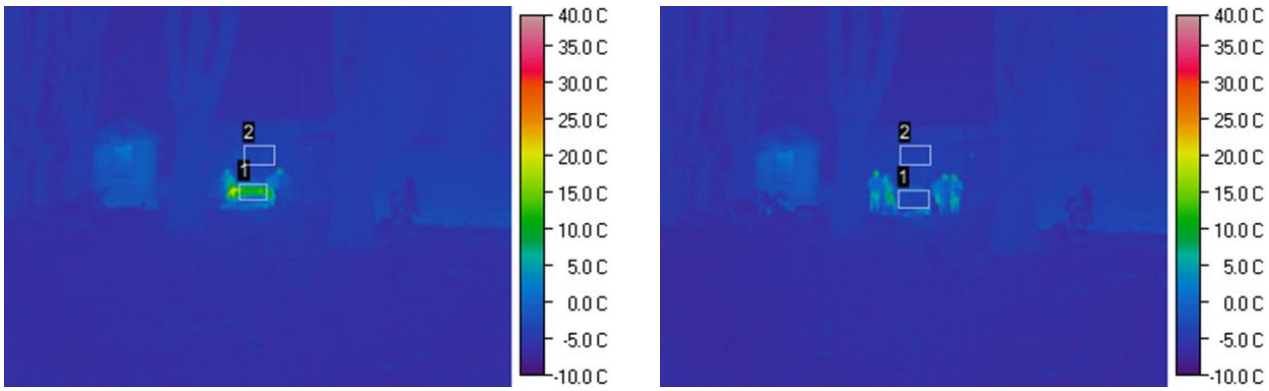

(a) (b)

Fig. 5. Thermal images of a warmed-up car without (a) and with (b) masking coating.

4. MDR for masking coatings

As an example of these approaches, we provide similar calculations for one of the human IR masking clothes, available on the market [15]. The minimal object dimension for humans was taken equal to 0.5 m. Fig. 4 presents the thermal images of a person reflecting the changes in his infrared emission due to using the thermal masking clothes. The ΔT for the unmasked person was equal to 4.7 K, and after covering him with the thermal clothes it became equal to 1.2 K. It should be noted that the measurements were carried out in summer, which resulted in a relatively high background temperature. In cold weather, results should differ due to much lower background temperature.

We performed the same calculations as presented in Figs 1 and 2, and found that for ideal conditions (uniform background) changes in the MDR for a human being would be the following.

For 3…5 μm thermal imager and good weather conditions, covering a person with the thermal masking clothes decreases MDR from 12.2 to 9.6 km indicating a 21.3% decrease. For limited weather conditions, the thermal masking clothes decrease MDR from 4.68 to 3.64 km indicating a 22.2% decrease. For 8…12 μm thermal imager and good weather conditions, the thermal masking clothes decrease MDR from 1.89 to 1.43 km indicating a 24.3% decrease. For limited weather conditions, such clothes decrease MDR from 1.49 to 1.11 km indicating a 25.5% decrease.

Another important example is the thermal masking of a car. It usually has a sufficiently higher temperature contrast with the background, and depending on a car state (parked, parked with a warmed engine, driving, *etc*.) this contrast can change.

In contrast to the previous example, further thermal imaging was carried out during winter, which resulted in a lower background temperature and probably resulted in a higher temperature contrast for unmasked vehicles. The critical dimension for the car was taken equal to 2.3 m according to the NATO standard. Fig. 5 shows the infrared images of the car parked with the warmed engine. For the thermal masking of the car in Fig. 5b one of the specially designed coatings was used.

In Fig. 5 ΔT for the unmasked car is 9.9 K, while for the thermally camouflaged car, it is only 0.5 K. Similarly to the previous example, we used this data to model the MDR for this car in good and adverse weather conditions. For 3…5 μm thermal imager and good weather conditions, the MDR for the unmasked car is 25.8 km, while for the thermally camouflaged car – 14.4 km. For adverse weather conditions, the MDR for the unmasked car is 6.35 km, while for the thermally camouflaged car – 3.55 km. The MDR decreased by approximately 44.2% for both weather conditions. For 8…12 μm thermal imager and good weather conditions, the MDR for the unmasked car is 7.9 km, and for the thermally camouflaged car – 4.15 km. For adverse weather conditions, the MDR for the unmasked car is 3.95 km, while for the thermally camouflaged car – 2.07 km. Thus, in good weather, the MDR decreased by 47.5%, while in limited weather conditions – decreased by 47.6%. The weak variations in the decrease of MDR probably should be manifested in calculation errors.

In this case, the used thermal coating leads to more than an order of magnitude decrease in the temperature difference between the target and the background, which resulted in an almost twofold decrease in MDR.

5. Conclusions

As thermal signature reduction is a powerful technology against IR reconnaissance and can give advantages on the battlefield, it is drastically important to estimate its efficiency.

Thus in this work, we provided numerical estimations for the relative decrease of the MDR with lowering the target temperature contrast with the background. Although these estimations are based on the experimental MRTD measurements for two particular thermal imager models, they are carried out within the range of spatial frequencies and temperatures where the imager resolution is not limited neither by the NETD nor by the spatial resolution. Consequently, speaking about the relative decrease of the MDR due to the reduction in the target thermal signature, one can assume that these calculations could serve as a qualitative estimate for other thermal imager models in the same conditions.

These estimations can be used for the characterization of thermal masking coatings available on the market, allowing one to connect the observed decrease of a target temperature contrast ΔT with the decrease in its MDR. The benchmark estimations have shown that the decrease of ΔT by an order of magnitude leads to the decrease of MDR by approximately one-third. At the same time, the decrease in ΔT by two orders of magnitude leads to the decrease of the MDR by approximately two-thirds. This result is valid within both 3…5 and 8…12 μm spectral ranges. Presented numerical estimation allows one to suggest that aforementioned relative decrease of MDR does not depend on weather conditions.

Also, we carried out experimental and numerical studies of several thermal coatings available on the market, one for personnel and another one for a car, and ascertained that the obtained decrease in the MDR is close to one-fourth for personnel and close to one-half for a car.

These estimations are based on the assumption of a uniform background temperature and correspond to the maximal possible detection range of thermal imagers and are valid in these conditions only. In the non-uniform background temperature conditions, the real MDR could be smaller and could change differently with the use of a thermal signature reduction. The latter strongly depends on the background temperature pattern, coloring of target camouflage, illumination, *etc*., and cannot be summarized into simple estimates.

Acknowledgments

This study was supported by NRFU project #2023.04/0026. The authors are sincerely grateful to all defenders of Ukraine and emergency workers who made possible publication of the research results.

References

1. Barela J., Firmanty K., Kastek M. Measurement and analysis of the parameters of modern long-range thermal imaging cameras. *Sensors*. 2021. **21**. P. 5700. https://doi.org/10.3390/s21175700.
2. Perić D., Livada B., Perić M., Vujić S. Thermal imager range: Predictions, expectations, and reality. *Sensors*. 2019. **19**, No 15. P. 3313. https://doi.org/10.3390/s19153313.
3. Krišto M., Ivasic-Kos M. and Pobar M. Thermal object detection in difficult weather conditions using YOLO. *IEEE Access*. 2020. **8**. P. 125459–125476. https://doi.org/10.1109/ACCESS.2020.3007481.
4. Chrzanowski K. Testing surveillance thermal imagers under simulated real work conditions. *Opto-Electron. Rev.* 2023. **31**. P. e145327. https://doi.org/10.24425/10.24425/opelre.2023.145327.
5. Wu Y., Tan S., Zhao Y. *et al.* Broadband multispectral compatible absorbers for radar, infrared and visible stealth application. *Prog. Mater. Sci*. 2023. **135**. P. 101088. https://doi.org/10.1016/j.pmatsci.2023.101088.
6. Sizov F.F. Brief history of THz and IR technologies. *SPQEO*. 2019. **22**. P. 67–79. https://doi.org/10.15407/spqeo22.01.067.
7. Gustafsson O., Glendor P. Infrared signature simulations of a mobile camouflage for a heavy military vehicle. *Proc. SPIE*. 2019. **11158**. P. 111580D-1. https://doi.org/10.1117/12.2533452.
8. Melezhyk Ye.O., Tsybrii Z.F., Zabudsky V.V. *et al.* Evaluating benchmarks for the effectiveness of infrared camouflage coatings. *Bogolyubov Kyiv Conference "Problems of Theoretical and Mathematical Physics"*, 24–26 September 2024.
9. *NATO Standardization Agreement 4347*, Definition of nominal static range performance for thermal imaging systems, Military Agency for Standardization (1995).
10. Johnson J. Analysis of imaging forming systems. In: *Proceedings of the Image Intensifier Symposium*, Ford Belvoir, VA, USA, 6–7, October 1958; U.S. Army Engineer Research and Development Lab.: Ford Belvoir, VA, USA, 1958. P. 249–273.
11. Melezhik Ye.O., Sizov F.F., Shevchyk O.V., Gumenjuk-Sichevska J.V. Methods of numerical simulation of the IR radiation of gas turbine engines to evaluate the possibility of reducing the visibility of aircrafts. *Reports of the National Academy of Sciences of Ukraine*. 2020. **4**. P. 43–52. https://doi.org/10.15407/dopovidi2020.04.043.
12. Qin B., Zhu Y., Zhou Y. *et al*. Whole-infrared-band camouflage with dual-band radiative heat dissipation. *Light Sci. Appl*. 2023. **12**. P. 246. https://doi.org/10.1038/s41377-023-01287-z.
13. Chrzanowski K. *Testing Thermal Imagers*. Practical guidebook. Military University of Technology, Warsaw, Poland, 2010.
14. Kolobrodov V.G., Gordienko V.I., Mykytenko V.I. *et al*. *Scientific and Practical Aspects of Creation of Thermal Imaging Systems*. Cherkasy, Ukraine, Vertikal Publ., 2015 (in Ukrainian). https://ela.kpi.ua/handle/123456789/28022.
15. Degenstein L.M., Sameoto D., Hogan J.D. *et al*. Smart textiles for visible and IR camouflage application: State-of-the-art and microfabrication path forward. *Micromachines*. 2023. **12**. P. 773. https://doi.org/10.3390/mi12070773.

Authors and CV

Yevhen O. Melezhyk, PhD, Researcher at the V. Lashkaryov Institute of Semiconductor Physics. His research interests include numerical modelling of IR emission, IR absorption and propagation in gaseous medium, thermal imaging, HgCdTe heterostructures. E-mail emelezhik@gmail.com, https://orcid.org/0000-0001-6135-8231

Zinoviia F. Tsybrii, Doctor of Sciences, Head of Department at the V. Lashkaryov Institute of Semiconductor Physics. The area of her scientific interests includes physics and technology of semiconductor materials, heterostructures and devices (IR and THz detectors, nanomaterials, *etc*.). E-mail: tsybrii@isp.kiev.ua, http://orcid.org/0000-0003-1718-5569

Viacheslav V. Zabudsky, PhD, Senior Researcher at the V. Lashkaryov Institute of Semiconductor Physics. Field of research: development of testing equipment and methods, investigation of HgCdTe detection properties, IR and THz detectors, vision systems in IR and THz spectral regions. E-mail: zvv1968@yahoo.com, https://orcid.org/0000-0003-2033-8730

Nataliia I. Kukhtaruk, PhD, Researcher at the Department of IR and THz Electronics, V. Lashkaryov Institute of Semiconductor Physics. Field of research: IR and THz detectors and vision. https://orcid.org/0000-0002-2227-4921

Viktor V. Strelchuk, Doctor of Sciences, Professor, Leading Researcher at the Laboratory of Submicron Optical Spectroscopy, V. Lashkaryov Institute of Semiconductor Physics. Field of researches: physics of semiconductors, Raman and photoluminescence spectroscopy of semiconductors, nanostructures and nanoscale materials. E-mail: viktor.strelchuk@ccu-semicond.net, https://orcid.org/0000-0002-6894-1742

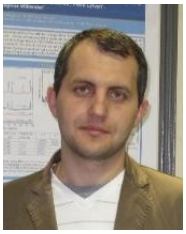

Andrii S. Nikolenko, PhD, Senior Researcher at the Submicron Optical Spectroscopy Laboratory, V. Lashkaryov Institute of Semiconductor Physics. Field of research: semiconductor nanostructures and heterostructures, Raman, photoluminescence and FTIR spectroscopy.
E-mail: nikolenko@isp.kiev.ua,
https://orcid.org/0000-0001-6775-3451

Oleksandr F. Kolomys, PhD, Senior Researcher at the Laboratory of Submicron Optical Spectroscopy, V. Lashkaryov Institute of Semiconductor Physics. Field of research: structural and optical study of semiconductor materials and nanostructures.
E-mail: olkolomys@gmail.com,
https://orcid.org/ 0000-0002-1902-4075

Vadym I. Popenko, PhD, Researcher at the V. Lashkaryov Institute of Semiconductor Physics. Field of research: optical, structural and electrical properties of carbon nanostructures and their composites with metals; Raman, photoluminescence and ellipsometry spectroscopy and XRD methods. E-mail: kurosavakata@gmail.com,
https://orcid.org/0009-0005-3116-9380

Denys M. Maziar, PhD student at the V. Lashkaryov Institute of Semiconductor Physics, NAS of Ukraine. The area of his research interests includes Raman spectroscopy and FTIR. Also interested in semiconductor thermoelectric converters.
E-mail: fmbfiz13.mazyar@kpnu.edu.ua,
https://orcid.org/0000-0002-8906-6107

Maksym A. Alieksandrov, PhD, Researcher at the Optics and Spectroscopy department, V. Lashkaryov Institute of Semiconductor Physics. Field of research: Raman spectroscopy, FTIR, mathematical modeling.
E-mail: mrmarafon@gmail.com,
https://orcid.org/0000-0002-9691-5170

Petro M. Lytvyn, PhD, Head of Department at the V. Lashkaryov Institute of Semiconductor Physics, NAS of Ukraine. His research focuses on solid-state physics, functional materials, and nanophysics of semiconductors and related materials. He has authored over 350 peer-reviewed publications, holds 10 patents, and has contributed to nine monographs, advancing knowledge in these fields.
E-mail: plyt@isp.kiev.ua,
https://orcid.org/0000-0002-0131-9860

Authors' contributions

Melezhyk Ye.O.: conceptualization, numerical calculation, writing – original draft.
Tsybrii Z.F.: conceptualization, writing – review & editing, validation.
Zabudsky V.V.: methodology, data curation, validation.
Kukhtaruk N.I.: methodology, data curation, validation.
Strelchuk V.V.: formal analysis.
Nikolenko A.S.: formal analysis.
Kolomys O.F.: formal analysis.
Popenko V.I.: formal analysis.
Maziar D.M.: formal analysis.
Alieksandrov M.A: formal analysis.
Lytvyn P.M.: conceptualization, methodology, writing – review & editing.

Чисельні оцінки максимальної відстані виявлення цілі в ІЧ-спектрі при зниженні температурного контрасту ціль-фон

Є.О. Мележик, З.Ф. Цибрій, В.В. Забудський, Н.І. Кухтарук, В.В. Стрельчук, А.С. Ніколенко, О.Ф. Коломис, В.І. Попенко, Д.М. Мазяр, М.А. Алєксандров, П.М. Литвин

Анотація. У цій статті розглянуто межу відстані виявлення цілі в інфрачервоному (ІЧ) спектрі для цілей з різними температурами. Наведено чисельні оцінки відносного зменшення максимальної дальності виявлення (МДВ) зі зменшенням температурного контрасту цілі відносно фону (ΔT). Показано, що зниження ΔT на порядок величини приводить до зниження МДВ приблизно на одну третину, тоді як зменшення на два порядки величини ΔT приводить до зниження МДВ приблизно на дві третини. Оцінки МДВ зроблено для сприятливих і несприятливих погодних умов. Ці результати відносно достовірні як для спектральних діапазонів 3…5 мкм, так і для 8…12 мкм і, схоже, не залежать від погодних умов.

Ключові слова: ІЧ, тепловий контраст, максимальна дальність виявлення.